Energy & Environmental Science

Accepted Manuscript

This article can be cited before page numbers have been issued, to do this please use: C. Xu, P. Jing, P. Xia, Y. Jia, J. Peng, Q. He, Q. Liu, Z. Song, X. Zhang, F. Wu, X. Liu, K. Wu, W. Cai and Y. Zhang, *Energy Environ. Sci.*, 2025, DOI: 10.1039/D5EE02060C.

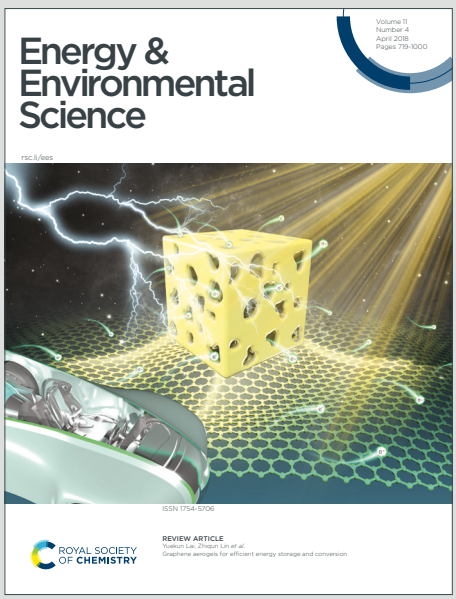

ROYAL SOCIETY OF CHEMISTRY

rsc.li/ees

View Article Online
DOI: 10.1039/D5EE02060C

Broader context

Despite great achievements that have been made by designing bilayer solid electrolyte interphase (SEI), it still remains a tremendous challenge to further improve the mechanical properties and ion diffusion kinetics of the SEI layer on Si-based materials. In this work, we innovatively designed a fine-grained SEI layer through a meticulously controlled pulsed electrochemical activation strategy, marking the first application of this approach to optimize the electrochemical kinetics and long-term stability of Si/C anodes. By precisely modulating the pulse parameters, the multiple-layer fine-grained SEI is well constructed and consists of uniform fine inorganic particles (such as LiF and Li3N) in each layer and interspersed with buffer oligomer organics. Benefiting from the fine-grain strengthening effect, the constructed SEI not only features enhanced rigidity and flexibility characteristics to accommodate the volume changes, but also achieves a much smaller Gibbs free energy to promote Li^+ diffusion kinetics. Notably, this pulsed electrochemical activation maneuver bridging the gap between fundamental interfacial science and practical battery applications not only offers a novel and scalable pathway for interface engineering, but also presents a promising and industrially viable strategy for improving cycle stability in commercial lithium-ion batteries.

View Article Online
DOI: 10.1039/D5EE02060C

ARTICLE

Tailoring Multilayer Fine-Grained Solid Electrolyte Interphase by Pulse Electrochemical Activation Maneuver for Stable Si/C Anodes†

Changhaoyue Xu,[a] Peng Jing,[a] Pengfei Xia,[a] Ye Jia,[a] Jianan Peng,[a] Qiujie He,[a] Qingqing Liu,[b] Zimo Song,[a] Xuemei Zhang,[c] Fanglin Wu,[d] Xianyu Liu,[e] Kaipeng Wu,[a,f] Yun Zhang,[a,f*] and Wenlong Cai[a,f*]

Received 00th January 20xx,
Accepted 00th January 20xx

DOI: 10.1039/x0xx00000x

Silicon (Si) is widely regarded as one of the most promising anode materials for lithium-ion batteries due to its exceptionally high specific capacity. However, the significant volumetric changes (up to 400%) of Si anode degrades the solid-electrolyte interphase (SEI) and significantly hinders its practical application. Herein, we modulate the formation of fine-grained SEI composed of multiple layers by pulse electrochemical activation mode, where each layer is uniformly distributed with fine inorganic particles and interspersed with buffer organics. This tailored multilayer fine-grained SEI effectively promotes the lithium-ion diffusion kinetics through SEI featuring a small Gibbs free energy (0.235 eV), which is only 1/5 of the typical double-layer SEI, as well as smaller charge transfer resistances during the whole electrochemical processes. Moreover, it exhibits a high Young's modulus of 12.5 GPa in comparison to that of the typical double-layer SEI (5.1 GPa) and much-inhibited stress and strain, so as to generate lower thickness expansion/shrinkage ratios. Consequently, the assembled Si/C || $LiFePO_4$ full cell, operating at a current density of 1 A g^{-1}, demonstrates a remarkable capacity retention of 93.6% after 583 cycles, which also shows a practical application by powering an unmanned aircraft. This interfacial engineering maneuver sheds light on enhancing the electrochemical performance of other high-capacity electrode materials with substantial volume changes.

Introduction

Driven by social progress, the demand for environmentally friendly, high-capacity batteries is growing, and silicon (Si) stands out of the anode materials due to its high theoretical specific capacity (4200 mAh g^{-1}).[1, 2] However, the substantial volumetric expansion (approximately 400%) leads to the vital solid-electrolyte interphase (SEI) continuously reshaping, resulting in electrolyte depletion and loss of active materials.[3, 4] Constructing stable SEI layers to maintain the Si particle integrity has been demonstrated as an efficient method, which has made a great stride. Research in this area has primarily focused on two key strategies: firstly, pre-constructing an artificial coating layer on the surface of Si-based materials to serve as the SEI film, isolating the active material from direct contact with the electrolyte, and mitigating undesirable side reactions.[5-7] The second approach involves optimizing the electrolyte composition to enable the *in-situ* formation of a stable SEI film by electrochemical methods, including the use of electrolyte additives[8-11] and novel electrolyte systems[12-16].

To date, substantial efforts have been devoted to exploring strategies to modulate the electrolyte solvation structure to construct a unique SEI structure. It has been acknowledged that the ideal SEI possesses a bilayer structure, characterized by an inorganic inner layer and an organic outer layer, which has been extensively validated in lithium metal and graphite anodes.[17, 18] By modulating the type and concentration of the solvent, the formation of the solvation structure can be precisely controlled, thereby influencing the characteristics of the SEI.[19] Specifically, to construct the anion-enriched solvation structure, the double-layer SEI was intentionally constructed.[20-25] Except for electrolyte engineering, electrochemical strategies have also been proven to generate a LiF [26, 27] or *t*-Li_2ZrF_6-rich[1] interfacial layer without significantly changing the solvation structure, which could markedly accelerate Li-ion transfer and suppress the growth of Li dendrites. However, our recent research[28]

[a] *Department of Advanced Energy Materials, College of Materials Science and Engineering, Sichuan University, Chengdu, 610064, China.*
[b] *College of Polymer Science & Engineering, State Key Laboratory of Polymer Materials Engineering, Sichuan University, Chengdu, 610064, China.*
[c] *Institute of Smart City and Intelligent Transportation, Southwest Jiaotong University, Chengdu, 610032, China.*
[d] *State Key Laboratory of Advanced Technology for Materials Synthesis and Processing, Wuhan University of Technology, Wuhan 430070, China.*
[e] *Bailie School of Petroleum Engineering, Lanzhou City University, Lanzhou 730070, China.*
[f] *Engineering Research Center of Alternative Energy Materials and Devices, Sichuan University, Chengdu 610064, China.*
Email Address: caiwl@scu.edu.cn and y_zhang@scu.edu.cn
†Electronic Supplementary Information (ESI) available: [details of any supplementary information available should be included here].
See DOI: 10.1039/x0xx00000x

View Article Online
DOI: 10.1039/D5EE02060C

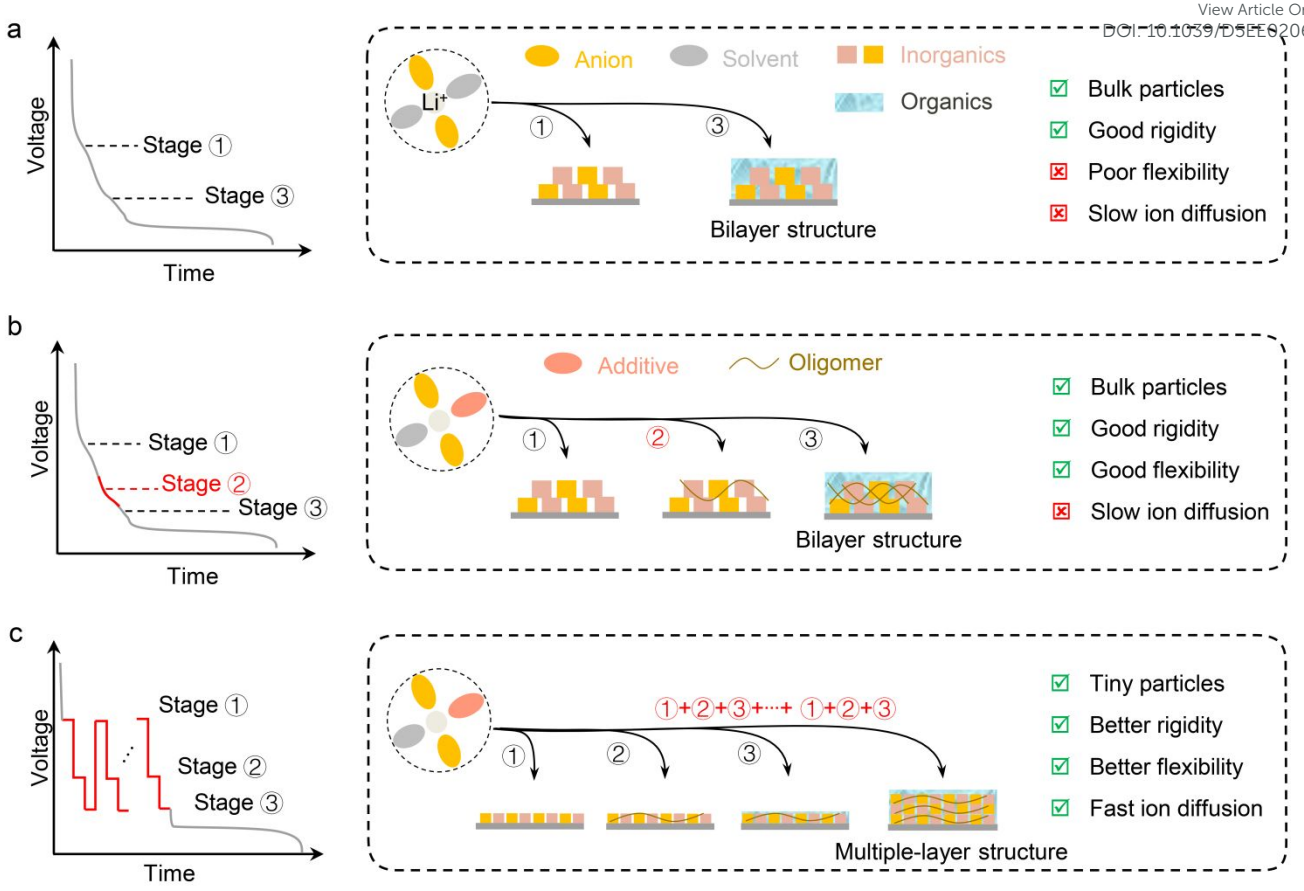

Fig. 1 Different SEI structures constructed by different electrochemical activation methods. (a) SEI formation by linear cyclic voltammetry with an anion-enriched solvation structure; (b)SEI formation by linear cyclic voltammetry with an anion-enriched solvation structure with additives; (c) SEI formation by the pulse voltage intervention with an anion-enriched solvation structure with additives

has revealed that incorporating oligomer layers to anchor inorganic particles is available to accommodate destructive volume expansion of Si anodes to maintain interphase stability. Despite these advances, the large particle size and non-uniform distribution of inorganic components may still exhibit a large lithium-ion (Li^+) diffusion barrier within SEI.[29-31] In this regard, Wang *et al.* pointed out that downscaling the crystal size of the electrode materials is the essential parameter to diminish the lithiation kinetics.[30] The smaller grain sizes with a larger grain boundary area as preferential channels for Li^+ migration. Therefore, the reduced diffusion distance and energy barrier of Li^+ is conducive to enhancing the diffusion kinetics during the electrochemistry process. Similarly, finer grains have also been shown to contribute to the synergistic effect of high strength and good ductility for most metallic materials to accommodate stress and strain.[32, 33] And when applied to lithium-ion batteries (LIBs), the fine-grained cathode and anode materials can effectively enhance the specific surface area, reduce the ion diffusion path, and improve the structural stability.[34, 35] How about exploring the ion diffusion kinetics and electrochemical performance by tailoring a fine-grained SEI on the Si surface, an approach that has never been considered?

Herein, a multilayer fine-grained SEI layer was first proposed to construct on Si surface by pulse electrochemical activation mode. By precisely regulating the decomposition potentials of individual electrolyte components and the growth time of inorganic species in each layer, the grain size can be controlled and uniformly distributed within the organic matrix of each SEI layer. The fine-grained SEI consists of multiple layers, with small inorganic particles evenly distributed from the inside out, bonded with flexible organic components. Moreover, the multilayer fine-grained SEI offered uniform ionic pathways, thereby obtaining a lower Li^+ diffusion barrier, which is only $1/5$ of the typical double-layer SEI. Additionally, Young's modulus of the multilayer fine-grained SEI is 12.5 GPa, significantly higher than that of the typical double-layer SEI (5.1 GPa). The strengthened rigidity and flexibility characteristics enhanced the structural stability of SEI and enabled it to accommodate the huge volume expansion of the Si anode during cycling. The feasibility of this approach has been rigorously examined through both experimental characterizations and theoretical analysis, with further studies into the interface properties and Li^+ diffusion mechanisms after grain refinement. To be specific, the Si/C anode exhibits excellent capacity retention (84.5%) after 400 cycles at a loading of 3 mg cm^{-2}. Further, the Si/C || $LiFePO_4$ full battery remains at 93.6% of its capacity after 583 cycles at a current density of 1 A g^{-1}.

Results and discussion

Multilayer Fine-grained SEI structure design

The electrochemical performance of Si-based anodes is primarily influenced by both the composition and structure of SEI. It is generally accepted that the anion-enriched solvation structure is able to generate classical SEI bilayer structures through two-step reduction, the anion reduction at a high plateau (stage ①) and solvent reduction at the low voltage (stage ③) (Fig. 1a).[36, 37] While the increased inner bulk inorganic components provide good rigidity, the incompatible organic polymers fail to effectively bind the nonadjacent bulk inorganic material together. This results in low Li^+ diffusivity and poor flexibility, which hampers its ability to accommodate the huge volume expansion of the Si anode during long-term cycling.[38] Recently, the additive was deliberately introduced to participate in an anion solvation sheath to generate low molecular weight oligomers after anion reduction (stage ②) (Fig. 1b).[28] The short-chain structure of oligomers facilitates the binding of bulk inorganic species, making the SEI structure both rigid and flexible. This enables the SEI to better adapt to the volumetric expansion of the Si anode during cycling.

However, the presence of such large inorganic particles will result in low Li^+ diffusivity. To address this issue, we hypothesize constructing fine-grained inorganic particles constituted SEI layer by optimizing the electrochemical activation method. Theoretically, different electrochemical reactions occur under different potential conditions. Thereupon, we deliberately manipulate the growth behavior of inorganic and organic species by controlling the voltage and reaction time during the reduction process (Fig. 1c). To be expected, the resultant multilayer fine-grained SEI exhibits improved rigidity and flexibility, allowing it to better accommodate the significant volumetric expansion of the Si anode during long-term cycling. More importantly, the numerous fine-grained interfaces are beneficial to boost ion diffusion kinetics. A kind of localized high-concentration electrolyte with 10% fluoroethylene carbonate (FEC) and 5% lithium nitrate ($LiNO_3$) additives (LHCE-FL) has been proven to produce bilayer structures with oligomers with good rigidity and flexibility.[39, 40] Herein, LHCE-FL is also used as a proof-of-concept, while the molecular aggregation states and the molecular dynamics snapshots are depicted in Fig. 2a and S1, respectively. Density functional theory (DFT) calculations then compare the activation energy changes of dimethyl ether (DME), FEC, lithium bis(fluorosulfonyl)imide (LiFSI), and $LiNO_3$, as well as their theoretical decomposition voltages (Fig. 2b and S2). Clearly, the lithium salts, $LiNO_3$ and LiFSI, are the first batch to be reduced to inorganic Li_3N and LiF at above 1.4 V, while FEC and DME are prone to generate oligomers and high molecular weight polymers at about 1.1 and 0.8 V. Then, linear sweep voltammetry (LSV) was conducted on Si/C anode to ascertain the decomposition voltages of each ingredient. As shown in Fig. 2c, there are three obvious dI/dV peaks, located between 1.28–1.51, 0.90–1.12, and 0.75–0.85 V consistent with the results of LSV (Fig. S3), corresponding to different electrochemical reduction processes. To more precisely confirm the optimal decomposition voltages, discharging at a constant voltage is adopted to compare the coulombic efficiency (CE) of the reversible capacity (Fig. 2d). Specifically, it was found that the constant voltages at 1.4, 1.0, and 0.8 V correspond to the highest CE for each respective stage, as shown in Fig. 2e and Fig. S4–S6.

Based on the above results, a pulse constant voltage decomposition experiment was designed, as shown in Fig. 2f. The SEI was constructed at the decomposition voltages of $LiNO_3$/LiFSI (1.4 V), FEC (1.0 V), and DME (0.8 V), respectively, for a short time. And then repeated several times to control the grain particle size, which is referred to as "consSEI-xth", where x indicates the number of repeating times. For comparison, the common electrochemical method to construct SEI layer is referred to as "w/o consSEI". The differences in the initial CE and discharge capacity are obvious with constructing different times, as depicted in Fig. 2g and Fig. S7–S11, where the Si/C electrode with consSEI-100th shows the highest average initial CE and capacity of 86.3% and 1244 mAh g^{-1}. Furthermore, consSEI-100th maintains the highest specific discharge capacity even after 100 cycles at a current density of 1 A g^{-1} (Fig. 2h).

Morphology and structure analysis of SEI layer

The unique structure of the multilayer fine-grained SEI on Si/C anode is then investigated. Cryo-transmission electron microscopy (Cryo--TEM) in Fig. S12 reveals the typical bilayer structure of w/o consSEI, consisting of an inorganic inner layer and an organic outer layer. In comparison, the consSEI-xth shows superimposed structures, while the more repeating times, the more superimposed layers (Fig. 3a, S13–S14). Furthermore, as confirmed by electron diffraction (Fig. 3b and S13b), it is evident that $LiNO_3$/LiFSI decompose to form the inorganic components Li_3N and LiF during SEI construction, and these materials are present in each layer of the SEI. As expected, the consSEI-100th features a layered structure with small Li_3N and LiF particles present in each SEI layer, as shown in Fig. 3c, while w/o consSEI shows larger inorganic particles in inner side for comparison (Fig. 3d). This suggests that the pulse electrochemical method of consSEI-100th forms a fine-grained SEI layer with a multilayered structure distinct from that of w/o consSEI.

To further investigate the regulatory effect of consSEI-100th on SEI components at the Si/C anode surface, the interface composition after SEI construction was analyzed using X-ray photoelectron spectroscopy (XPS). Before that, the decomposition products at different voltages are validated. Fig. S15a and S15d show that $LiNO_3$ and LiFSI decompose at 1.4 V, their highest concentrations of Li_3N and LiF indicate much organics is produced at this voltage. Sweeping to 1.0 V (Fig. S15b and S15e), the ratios of Li_3N and LiN_xO_y of N 1s decrease, while the ratio of LiF barely changes suggesting that some inorganic compounds are also generated during FEC decomposition. Finally, at 0.8 V (Fig. S15c and S15f), where DME decomposes to only produce organic materials, the ratio of LiF in F 1s and that of Li_3N and LiN_xO_y in N 1s all decreases.

To further validate our hypothesis regarding the construction of multilayer fine-grained SEI, we conducted an in-depth analysis of the interphase during the formation process using *ex-situ* XPS.

View Article Online
DOI: 10.1039/D5EE02060C

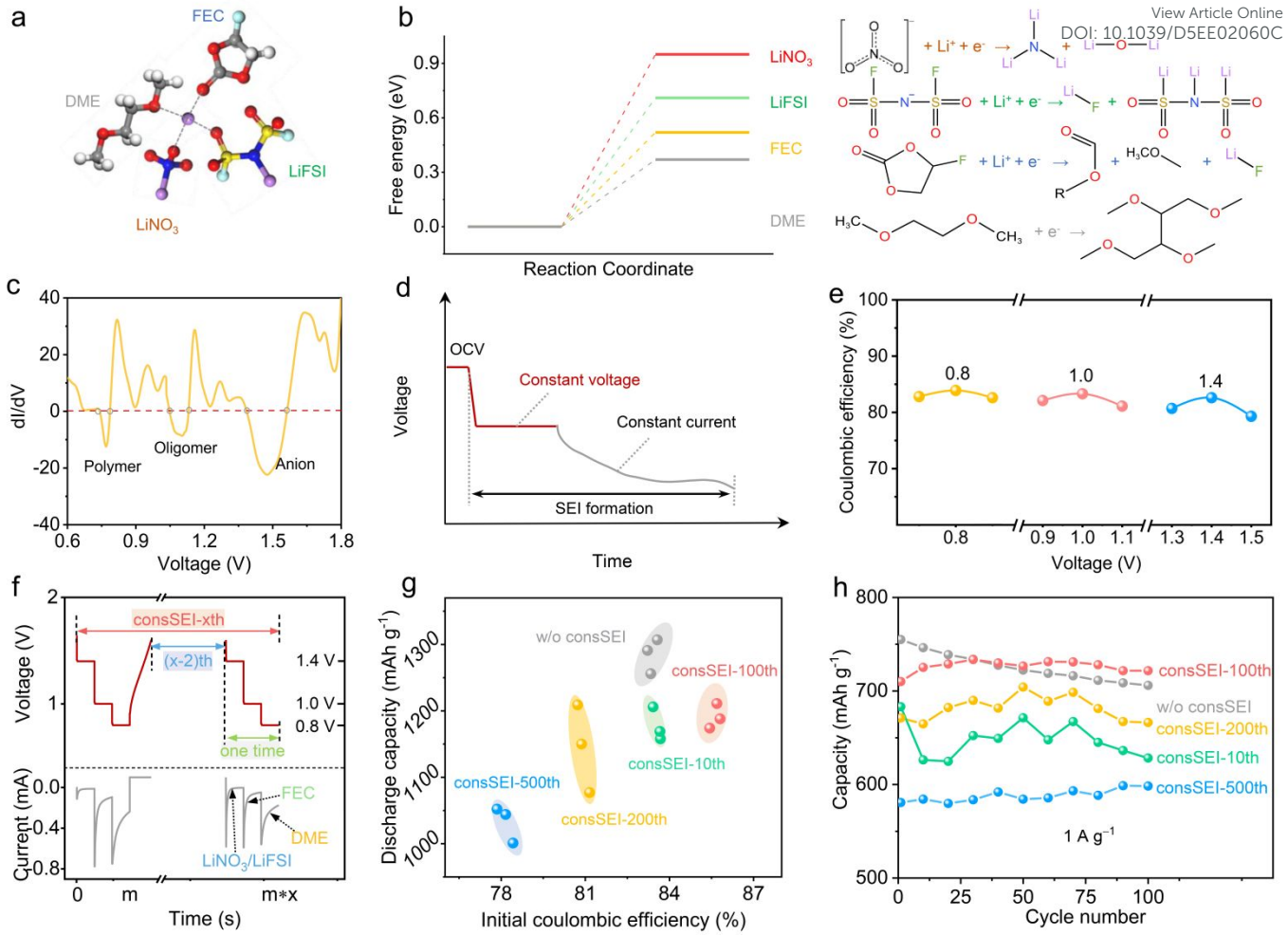

Fig. 2 The design principle for constructing a fine-grained SEI layer. (a) The solvation structure of LHCE-FL electrolyte based on molecular dynamics simulation; (b) Different activation energies for decomposition of $LiNO_3$, LiFSI, FEC, DME, and corresponding de-composition reactions; (c) The derived dI/dV–voltage curves from LSV; (d) The schematic of constant voltage discharging and corresponding (e) coulombic efficiency; (f) The schematic of designed pulse constant voltage discharging and corresponding (g) initial coulombic efficiency and discharge capacities, and (h) long-term cycling performance.

And the changes in SEI composition during the voltage transitions in the initial cycle from open-circuit voltage skipping to 1.4 V (Stage 1), then to 1.0 V (Stage 1 to 2), and finally to 0.8 V (Stage 1 to 2 to 3) were analyzed. Fig. S16 has carried out the normalization and it shows that with increasing construction stages, the organic is formed so as the content of LiF and Li_3N decreases, indicating that each SEI layer is composed of inorganics wrapped in organics. Additionally, the SEI structure of consSEI-100th was analyzed by XPS and Ar^+ sputtering depth profiling. Fig. 3e and 3f demonstrate that, with increasing Ar^+ sputtering time, the organic and inorganic components of the SEI remain almost consistent, indicating uniform distribution across each SEI layer. Time-of-flight secondary ion mass spectrometry (TOF-SIMS) also indicates the uniform spatial distribution of the different SEI components. The three-dimensional images in Fig. 3g, along with Fig.S17 and 3h, show little variation in the spatial distribution of inorganic LiF_2^-, LiN^-, and organic fragments such as CHO_2^- and CH_3O^-. This indicates that the oligomers derived from FEC and the organic components produced by DME decomposition are uniformly within the SEI, interwoven with the inorganic Li_3N and LiF to form a stable and intertwined structure.[23,41]

Furthermore, Fig. 3i illustrates the close correlation between the inorganic LiF_2^-, LiN^-, and organic fragments (CHO_2^- and CH_3O^-) in SEI layer. This phenomenon can be attributed to the formation of the multilayer fine-grained SEI, wherein the smaller grain size facilitates an increased number of reaction sites. Consequently, the composition within each layer of the SEI is more uniformly distributed, leading to stronger correlations among individual components.

Advantages of the multilayer fine-grained SEI layer

Theoretically, the SEI with inorganic particles of varying sizes significantly influences the ion diffusion kinetics. As the grain size is refined to create a higher number of grain boundaries, the diffusion path is significantly shortened, allowing Li^+ to move more easily through the SEI (Fig. 4a), which is beneficial to enhance the rate capability. Then, to investigate the mechanism behind the multilayer fine-grained SEI layer of consSEI-100th, the Li^+ diffusion energy barrier for both w/o consSEI and consSEI-100th was calculated using first principles. Due to the increased grain boundary contact between Li_3N and LiF in consSEI-100th (Fig. S18), the energy barrier is 0.235 eV

View Article Online
DOI: 10.1039/D5EE02060C

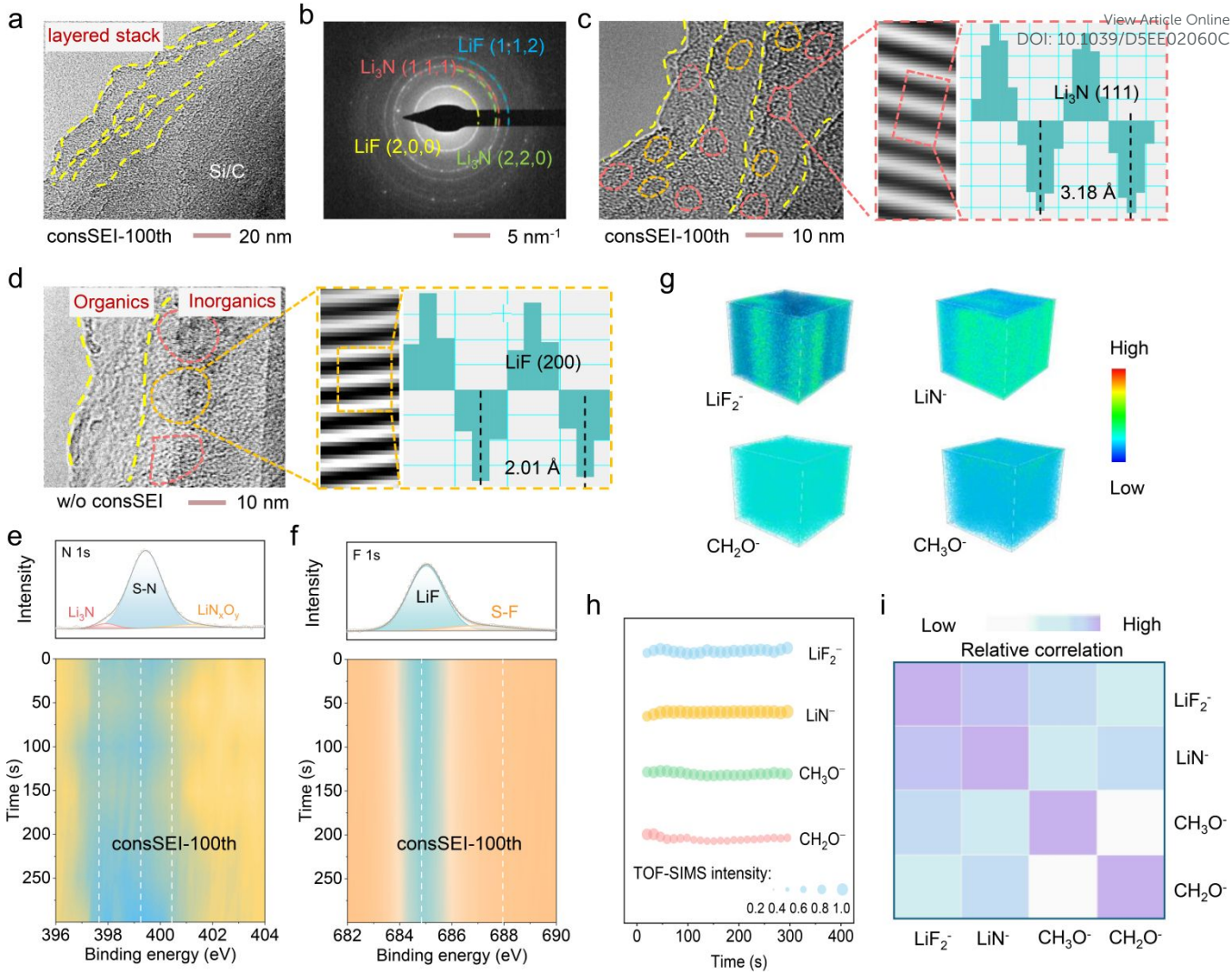

Fig. 3 Morphology and composition analysis of the multilayer fine-grained SEI layer. (a) Cryo-TEM images of SEI in consSEI-100th; (b) Selected-area electron diffraction of SEI in consSEI-100th; magnified HRTEM images and corresponding FFT images of SEI in (c) consSEI-100th (d) w/o consSEI; Depth sputtering (e) N 1s and (f) F 1s XPS contour plots of the Si/C anode after cycling in consSEI-100th; (g) 3D TOF-SIMS sputtering images and the selected secondary ion fragments (LiF_2^-, LiN^-, CHO_2^- and CH_3O^-) of the cycled Si/C anode in consSEI-100th and corresponding (h) normalized (to maximum) TOF-SIMS depth profiles of characteristic fragments; (i) Relative correlation matrix for the fragments of interest (LiF_2^-, LiN^-, CHO_2^- and CH_3O^-).

for consSEI-100th as illustrated in Fig. 4c, which is much lower than that for w/o consSEI in Fig. 4b (1.078 eV). The lower diffusion energy barrier in consSEI-100th indicates more efficient ion transportation. To verify this, *in-situ* electrochemical impedance spectroscopy (EIS) was used to analyze the charge transfer kinetics (Fig. S19). By converting the EIS data into a relaxation time distribution function in the time domain, a continuous curve with distinct peaks, where each one corresponds to a specific dynamic process, can be obtained. As shown in Fig. S20, the peak around 10^{-5} –10^{-3} s corresponds to the ohmic internal resistance (R_{ob}), while that at 10^{-3} –10^{-2} s and 10^{-2}–10^{-1} s corresponds to the ohmic impedance (R_{SEI}) and the charge transfer impedance (R_{ct}).[42] Clearly in Fig. 4d, the R_{ct} during the whole Si/C alloying and dealloying reaction for w/o consSEI is consistently higher than that for consSEI-100th. Furthermore, the diffusion behavior of Li^+ in different Si/C electrodes was compared by galvanostatic intermittent titration technique (GITT), and the Li^+ diffusion coefficient ($\mathbf{D}_{Li^+}$) was calculated using equation (1):[43-47]

$$\mathbf{D}_{Li^+} = \frac{4}{\pi\tau}\left(\frac{n_M V_M}{S}\right)^2\left(\frac{\Delta E_s}{\Delta E_\tau}\right)^2$$

where τ = 3600 s, n□ and V□ are the molar and molar volume of Si/C, and the electrode area is 1.13 cm^2. As depicted in Fig. S21, the calculated average $\mathbf{D}_{Li^+}$ for consSEI-100th during lithiation and de-lithiation is 4.53×10^{-10} cm^2s^{-1}, an order of magnitude higher than that for w/o consSEI (5.51×10^{-11} cm^2s^{-1}). These results indicate that the multilayer fine-grained SEI is beneficial in reducing interfacial and charge transfer resistances, leading to enhanced electrochemical performance.

To further examine the effect of SEI grain refinement on the stress and strain of the Si/C anode, finite element simulations were

View Article Online
DOI: 10.1039/D5EE02060C

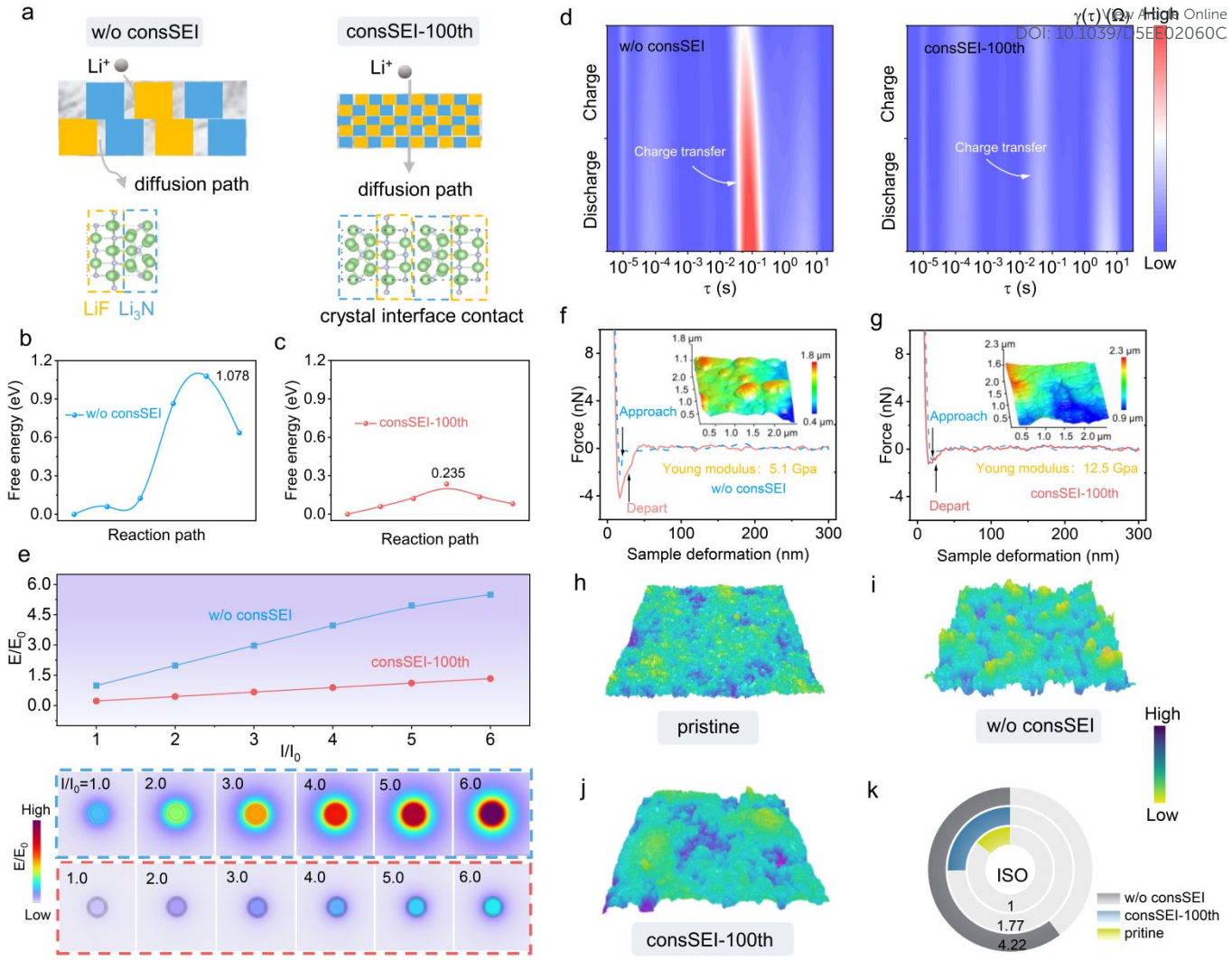

Fig. 4 Dynamic performance and interphase characterizations. (a) Schematic diagram of Li^+ diffusion in the fine-grained SEI layer; Gibbs free energy of Li^+ diffusion path in (b) w/o consSEI and (c) consSEI-100th model; (d) DRT impedance spectra of the Si/C electrode with consSEI-100th and w/o consSEI; (e) The electric field intensity distribution, the changes of the maximum electric field intensity for w/o consSEI and consSEI-100th models at different current densities, the effects of stress engineering by the COMSOL modeling; Quantitative nanomechanical mapping of the cycled Si/C anode with (f) w/o consSEI and (g) consSEI-100th, inset show the corresponding AFM morphologies; Spectral diagram of 3d profiler: (h) pristine, (i) w/o consSEI, (j) consSEI-100th, and corresponding (k) Roughness.

performed using COMSOL Multiphysics. The variation in current (I/I_o) and electric field intensity (E/E_o) were introduced to assess the stress and strain of the Si/C anode.[48, 49] Fig. S22 shows enlarged images of the original states for both w/o consSEI and consSEI-100th, where it is evident that the SEI structure on the surface of Si/C particles in consSEI-100th is more refined. As illustrated in Fig. 4e, the evolutions of the simulated electric field intensities both increase with the rising of current increases. Compared to consSEI-100th, the electric field strength for that with w/o consSEI is always more pronounced with increasing current, hinting at the enhanced stress and strain in the Si/C electrode to lead to severe structural damage and failure during repeated cycling.[50] This indicates that the consSEI-100th feature of the multilayer fine-grained SEI structure is more rigid and flexible, enabling it to better accommodate the volume expansion of the Si/C anode caused by Li-Si alloying/de-alloying behavior. For further exploring the impact of the multilayer fine-grained SEI on the physical properties of the Si/C anode surface, atomic force microscopy (AFM) was employed. As shown in Fig. 4f and 4g, the surface Young's modulus of the Si/C anode with consSEI-100th is 12.5 GPa, significantly higher than that of w/o consSEI (5.1 GPa). Moreover, comparing the morphology of the original state of the Si/C anode (Fig. S23) and high-resolution AFM images (Fig. S24), the morphological development of consSEI-100th is minimal in comparison with that of w/o consSEI. Finally, to investigate the overall state of the Si/C anode after SEI construction, 3D optical profilometry was also used. Fig. S25 shows that during SEI construction, the electrode surface becomes flatter as the SEI construction progresses, indicating the formation of organics with flexible properties gradually increases during the SEI

View Article Online
DOI: 10.1039/D5EE02060C

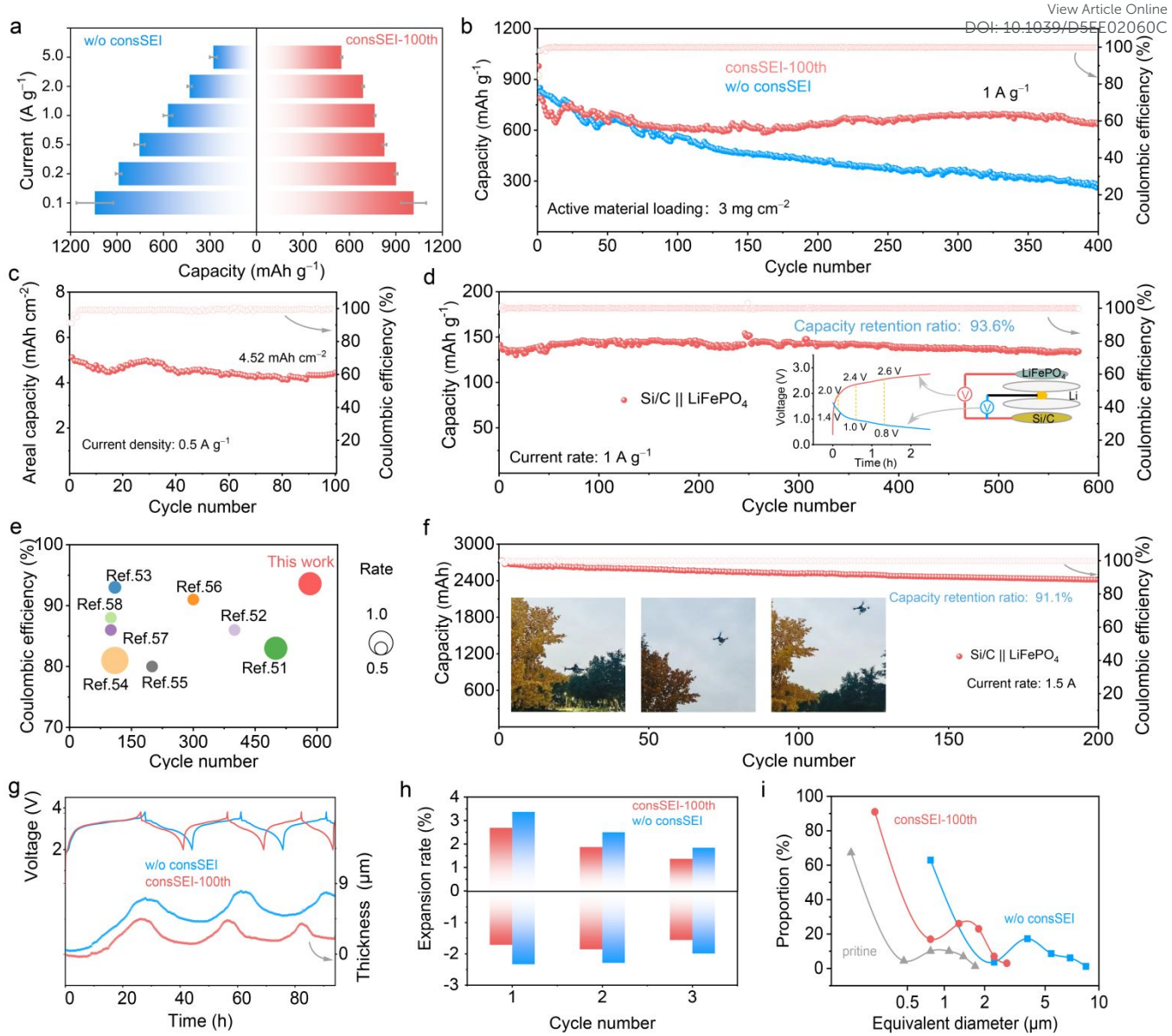

Fig. 5 Electrochemical performances of Si/C anodes with different SEI layers. (a) Comparison of the rate capabilities of Si/C anode with different SEI layers; (b) Cycling stabilities of Si/C anode with mass loading of 3 mg cm^{-2} at 1 A g^{-1}; (c) Cycling performance of the Si/C electrode with consSEI-100th at 0.5 A g^{-1}; (d) Long-term cycling stability of the Si/C electrode with consSEI-100th in the Si/C || $LiFePO_4$ coin-cell and (e) in comparison with previous works, the inset in (d) gives the three-electrode profile of the Si/C || $LiFePO_4$ full cells; (f) Cycling capability of the Si/C || $LiFePO_4$ pouch cell in consSEI-100th, the insets are the picture of this Si/C || $LiFePO_4$ pouch cell in drone application; (g) Thickness variation of the Si/C electrode during the charging and discharging process and corresponding (h) volume expansion rate; (i) Comparison of particle size of the Si/C composites before and after cycling.

construction process and provides the electrode with some flexibility and smoothness. Furthermore, Fig. 4h–j and S26 demonstrate that after cycling, the pole pieces of consSEI-100th are more uniform compared to the counterparts. To further quantify the flatness, Fig. 4k calculates that the roughness of the consSEI-100th electrode is reduced to 1.77 far less than w/o consSEI (4.22), and shows smoother characteristics. Therefore, it demonstrates that the multilayer fine-grained SEI possesses both excellent flexibility and rigidity, making it more adaptable to the significant volume expansion of Si/C anode during the cycling process.

Electrochemical performances

To verify the potential of *in-situ* construction of multilayer fine-grained SEI layers for practical LIBs, the electrochemical properties of the Si/C anode were investigated. Firstly, Li || Si/C half cells were prepared. Fig. S27 shows the initial charge and discharge curves at a current density of 0.1 A g^{-1}. As expected, the Si/C anode of consSEI-100th shows a lower initial discharge capacity of 1256 mAh g^{-1}, compared with that of w/o consSEI (~1321 mAh g^{-1}), which can be attributed to the construction of SEI before battery testing.

Then, the rate capabilities at various current densities of the Si/C anode with different SEI layers were compared. As seen in Fig. 5a, Si/C anodes with different SEI exhibit comparable discharge capacities at low current densities (0.1–0.5 A g^{-1}). However, with the rising of current density, the Si/C electrode with consSEI-100th shows the obviously enhanced specific capacity compared with the counterpart. Specifically, the Si/C anode with consSEI-100th could deliver a reversible capacity as high as 567 mAh g^{-1} even at 5 A g^{-1}, which is far beyond that with w/o consSEI (278 mAh g^{-1}). Their difference in rate performance obviously hints that the consSEI-100th could remarkably enhance the Li–Si electrochemistry kinetics. Fig. 5b then compares the long-cycling performance of the Si/C anode with different SEI layers at a mass loading of 3 mg cm^{-2}. After 400 cycles at a current density of 1 A g^{-1}, the Si/C anode of consSEI-100th exhibits an excellent capacity of 645 mAh g^{-1}, accompanied by a good capacity retention as high as 84.5%. As for the Si/C anode with w/o consSEI, it only delivers an inferior capacity of 283 mAh g^{-1} with a low retention of 44.3%. This is logically attributed to the enhanced mechanical strength of consSEI-100th, which not only effectively mitigates the volume expansion of Si/C particles, but also guarantees the structural integrity of the entire electrode during cycling. Moreover, the Si/C anode with consSEI-100th could afford an area capacity of 4.52 mAh cm^{-2} at 0.5 A g^{-1} with stable cycling for 100 cycles (Fig. 5c), highlighting the high reversibility of the Li–Si alloy/dealloying behavior.

To further assess the practical applicability of consSEI-100th, commercial zero strain $LiFePO_4$ cathodes and Si/C anodes were assembled into full batteries, and the performance of the coin cell was first tested. Prior to assembling the Si/C || $LiFePO_4$ cell, the practical potential for constructing the multilayer fine-grained SEI was determined by a self-made three-electrode (Si/C–Li–$LiFePO_4$) setup (Fig. S28). As shown in the inset of Fig. 5d, the pulse voltages for constructing multilayer fine-grained SEI are 2.0, 2.4, and 2.6 V, respectively, corresponding to 1.4, 1.0, and 0.8 V in the half cell. After constructing SEI 100 times (Fig. S29), the Si/C || $LiFePO_4$ full battery was then cycled. Fig. S30 shows the initial charge and discharge curve at 0.1 A g^{-1} with an initial CE of 96.2%. The long-term cycling performance of the Si/C || $LiFePO_4$ coin cell at a current density of 1 A g^{-1} was presented in Fig. 5d. As shown, the full cell delivers an ultra-stable cycling capability with a capacity retention of 93.6% after 583 cycles, while the coincide charge and discharge curves at different cycle numbers without apparent voltage polarization and capacity decay in Fig. S31 suggests good reversibility of electrochemical reaction. In comparison with the other recent studies on Si/C anodes,[51-58] the cycling capability presented in this work demonstrates obvious superiority (Fig. 5e and Table S1).

Encouraged by the impressive performance of the Si/C || $LiFePO_4$ coin-cell, a commercial Si/C || $LiFePO_4$ pouch cell (about 3.0 Ah) was used to further evaluate the practical potential of the multilayer fine-grained SEI. Fig. S32 shows the structural diagram of the Si/C || $LiFePO_4$ pouch cell. As seen, the Si/C || $LiFePO_4$ pouch cell achieves an initial CE of up to 94% at 0.1 A current (Fig. S33). At a current density of 1.5 A, the reversible capacity of the Si/C || $LiFePO_4$ pouch cell remains at 2.47 Ah even after 200 cycles, corresponding to the capacity retention of 91.1% (Fig. 5f). By viewing the charge and discharge curves of the Si/C || $LiFePO_4$ pouch cell, as shown in Fig. S34, it only shows a slight capacity decay without severe voltage drop after prolonging the cycle number, confirming the excellent unmanned aircraft practical potential of this SEI tailoring strategy in high-energy LIBs (the inset pictures of Fig. 5f). Furthermore, it demonstrates that the fine-grained SEI achieved by consSEI-100th exhibits a more uniform structure, thereby reducing interfacial charge transport resistance, enhancing Li^+ diffusion kinetics, and contributing to improved rate performance and energy efficiency of the battery. Additionally, this SEI possesses both rigidity and flexibility, enabling it to accommodate volume changes in electrode materials during charging and discharging processes, thus preventing SEI rupture and spalling.

To explore the in-depth reason for the cycling stability of the Si/C with consSEI-100th in half and full cells, an in-situ electrode thickness monitor and postmortem SEM technique were carried out to investigate the structure variation of electrodes and materials. Fig. 5g records the thickness–time curves of the Si/C electrode with w/o consSEI and consSEI-100th in Si/C || $LiFePO_4$ coin cell during charge and discharge. Clearly, the cell with consSEI-100th shows a smaller thickness expansion compared with that with w/o consSEI. By calculation, it is found that the thickness expansion/shrinkage ratios of the Si/C electrode with consSEI-100th are 2.6%/1.7%, 1.8%/1.8%, and 1.3%/1.5% in the first three cycles (Fig. 5h). However, for the Si/C electrode with w/o consSEI, the thickness expansion/shrinkage ratios are significantly enhanced. This thickness variation can also be observed by the postmortem cross-section SEM images (Fig. S35) and in-situ optical images (Fig. S36–37) of the cycled Si/C electrode. Furtherly, the surface morphology of the electrode was analyzed by SEM and in-situ optical to discover thickness of consSEI-100th varies less, which indicates consSEI-100th can maintain the particle stability and constrain the volume expansion of Si/C particles after cycling. Moreover, Fig. S38 provides the postmortem SEM images of three Si/C electrodes, while Fig. 5i gives the statistical result of the Si/C particles. Although the grain size of the Si/C in the consSEI-100th and w/o consSEI electrode shows obvious augmented compared to pristine, the grain size in the consSEI-100th electrode after cycling is obviously lower than that in the w/o consSEI. This result indicates that the fine-grained SEI structure in the consSEI-100th electrode with the characteristics of uniformity, rigidity, and flexibility can effectively accommodate the volume expansion of Si/C particles, which is in favor of avoiding the repeated construction of SEI layer and electrolyte deterioration, eventually ensuring the long-term cycling stability and lifespan of Si-based electrode.

Conclusion

In conclusion, we present a pulse electrochemical activation maneuver to form a multilayer fine-grained SEI structure on Si/C anode. This approach ensures a uniform distribution of tiny inorganic particles (LiF/Li_3N) and an interwoven organic buffer layer, resulting in a rigid yet flexible multi-layered SEI. As a result, this multilayer fine-grained SEI is able to accommodate the huge volume expansion of the Si-based anode during cycling, thereby maintaining the integrity of both the electrode sheet and particles. Comprehensive

characterization demonstrates the viability of our strategy, while DFT calculations reveal a reduced Li^+ diffusion energy barrier after grain refinement. Furthermore, mechanical analysis confirms that the improved rigid-flexible SEI structure effectively accommodates the Si anode's volume changes. Consequently, the multilayer fine-grained SEI maintains a very stable interphase and the Si-based anode exhibits excellent capacity retention (84.5%) after 400 cycles at a current density of 1 A g^{-1}. Furthermore, the Si/C || $LiFePO_4$ full battery retains 93.6% of its capacity after 583 cycles at a current density of 1 A g^{-1}. This work sheds valuable insights into the design of SEI structures for high-volume expansion electrode materials in high-energy secondary ion batteries.

Author Contributions

Y. Zhang and W. Cai conceived and designed the experiments. C. Xu prepared the materials and conducted the characterization of materials and batteries. F. Wu, X. Liu, Q. Liu, Y. Jia, X. Zhang, K. Wu, and Z. Song helped to synthesize materials. P. Xia., J. Peng, and Q. He helped to analyze materials. P. Jing designed the toy devices for the pouch cell powering demonstration. C. Xu wrote the manuscript. W. Cai edited the manuscript. All authors discussed the results and have given approval to the final version of the manuscript.

Conflicts of interest

There are no conflicts to declare.

Acknowledgements

This work was supported by the National Science Foundation of Sichuan Province (2023NSFSC1124), Fundamental Research Funds for the Central Universities (YJ2021141), and the Science and Technology Cooperation Special Fund of Sichuan University and Zigong City (2022CDZG-9). The authors would like to thank Shiyanjia lab (www.shiyanjia.com) for the support of TEM, SEM, and XPS characterization and eceshi (www.eceshi.com) for support of TOF-SIMS. Sensofar Tech（www.sensofar.com） for the support of 3D Optical Profile. The authors also appreciate Dr. Can Liu from the Central Lab of the College of Materials Science and Engineering in Sichuan University for the help with measurements.

References

1 Y.-F. Tian, S.-J. Tan, C. Yang, Y.-M. Zhao, D.-X. Xu, Z.-Y. Lu, G. Li, J.-Y. Li, X.-S. Zhang, C.-H. Zhang, J. Tang, Y. Zhao, F. Wang, R. Wen, Q. Xu and Y.-G. Guo, Nat. Commun., 2023, 14, 7247.
2 Q. Xu, T. Li, Z. Ju, G. Chen, D. Ye, G. I. N. Waterhouse, Y. Lu, X. Lai, G. Zhou, L. Guo, K. Yan, X. Tao, H. Li and Y. Qiu, Nature, 2025, 637, 339–346.
3 J. Wang and Y. Cui, Nat. Energy, 2020, 5, 361–362.
4 Q. Liu, X. Wei, C. Yang, C. Xu, W. Cai and F. Chen, Small, 2024, 20, 2403938.
5 Y. Cheng, Z. Wang, J. Chen, Y. Chen, X. Ke, D. Wu, Q. Zhang, Y. Zhu, X. Yang, M. Gu, Z. Guo and Z. Shi, Angew. Chem. Int. Ed., 2023, 62, e202305723.
6 J. Sun, S. Zhang, J. Li, B. Xie, J. Ma, S. Dong and G. Cui, Adv. Mater., 2023, 35, 2209404.
7 M. Qin, Z. Zeng, Q. Wu, H. Yan, M. Liu, Y. Wu, H. Zhang, S. Lei, S. Cheng and J. Xie, Energy. Environ. Sci., 2023, 16, 546-556.
8 H. Wang, S. Chen, Y. Li, Y. Liu, Q. Jing, X. Liu, Z. Liu and X. Zhang, Adv. Energy Mater., 2021, 11, 2101057.
9 J. Tan, J. Matz, P. Dong, J. Shen and M. Ye, Adv. Energy Mater., 2021, 11, 2100046.
10 Y. Ou, W. Hou, D. Zhu, C. Li, P. Zhou, X. Song, Y. Xia, Y. Lu, S. Yan, H. Zhou, Q. Cao, H. Zhou, H. Liu, X. Ma, Z. Liu, H. Xu and K. Liu, Energy. Environ. Sci., 2025, 18, 1464-1476.
11 H. Wang, J. Liu, J. He, S. Qi, M. Wu, F. Li, J. Huang, Y. Huang and J. Ma, eScience, 2022, 2, 557–565.
12 Y. Liu, Z. Jin, Z. Liu, H. Xu, F. Sun, X.-Q. Zhang, T. Chen and C. Wang, Angew. Chem. Int. Ed., 2024, 63, e202405802.
13 L. Liu, Z. Shadike, N. Wang, Y.-M.Chen and J.-L. Zhang, eScience, 2024, 4, 100268.
14 X. Zhang, Z. Deng, C. Xu, Y. Deng, Y. Jia, H. Luo, H. Wu, W.Cai, and Y. Zhang, Adv. Energy Mater. 2023, 13, 2302749.
15 Y.-Z Li, Science, 2017, 358, 506–510.
16 L.-X. Ma, T.-D. Chen, C.-X. Hai, S.-D. Dong, X. He, Q. Xu, H. Feng, A. Xin, J.-T. Chen and Y. Zhou, Tungsten, 2024, 6, 259–268.
17 Z. Deng, Y. Jia, Y. Deng, C. Xu, X. Zhang, Q. He, J. Peng, H. Wu and W. Cai, J. Energy Chem., 2024, 96, 282–290.
18 W. Cai, Y. Deng, Z. Deng, Y. Jia, Z. Li, X. Zhang, C. Xu, X.-Q. Zhang, Y. Zhang and Q. Zhang, Adv. Energy Mater. 2023, 13, 2301396.
19 Y. Quan, X. Cui, L. Hu, Y. Kong, X. Zhang, H. Liang, Y. Zhu, C. Wang, N. Zhang and S. Li, Carbon Neutral., 2024, 4, e184.
20 Y. Ko, J. Bae, G. Chen, M. A. Baird, J. Yan, L. Klivansky, D.-M. Kim, S. E. Trask, M.-T. F. Rodrigues, G. M. Carroll, N. R. Neale and B. A. Helms, ACS Energy Lett., 2024, 9, 3448–3455.
21 W. Zhang, M. Dong, K. Jiang, D. Yang, X. Tan, S. Zhai, R. Feng, N. Chen, G. King, H. Zhang, H. Zeng, H. Li, M. Antonietti and Z. Li, Nat. Commun., 2022, 13, 5348.
22 N. Wu, J. Shen, X. Zhou, S. Li, J. Li, G. Liu, D. Guo, W. Deng, C. Yuan, X. Liu and H. Hou, Adv. Energy Mater., 2025, 1, 2405729.
23 B. Jin, A. Dolocan, C. Liu, Z. Cui and A. Manthiram, Angew. Chem. Int. Ed., 2024, 63, e202408021.
24 B. Jagger and M. Pasta, Joule, 2023, 7, 2228–2244.
25 G.-X Lu, Q.-Q Qiao, M.-T Zhang, J.-S Zhang, S. Li, C.-B Jin, and Z. J. Hua, Sci. Adv., 2024, 10, 7348.
26 P. Bai, X. Ji, J. Zhang, W. Zhang, S. Hou, H. Su, M. Li, T. Deng, L. Cao, S. Liu, X. He, Y. Xu and C. Wang, Angew. Chem. Int. Ed., 2022, 61, e202202731.
27 T. Ma, Y. Ni, Q. Wang, W. Zhang, S. Jin, S. Zheng, X. Yang, Y. Hou, Z. Tao and J. Chen, Angew. Chem. Int. Ed., 2022, 61, e202207927.
28 C. Xu, P. Jing, Z. Deng, Q. Liu, Y. Jia, X. Zhang, Y. Deng, Y. Zhang and W. Cai, Energy Storage Mater., 2025, 74, 103911.
29 Y. Luo, J. V. Handy, T. Das, J. D. Ponis, R. Albers, Y.-H. Chiang, M. Pharr, B. J. Schultz, L. Gobbato, D. C. Brown, S. Chakraborty and S. Banerjee, Nat. Mater., 2024, 23, 960–968.
30 R. Wang, L. Wang, R. Liu, X. Li, Y. Wu and F. Ran, ACS Nano, 2024, 18, 2611–31
31 X. Wang, A. Yu, T. Jiang, S. Yuan, Q. Fan, Q. Xu, Adv. Mater. 2024, 36, 2410482.
32 F. Xing, S. Liao, J. Qin, G. Wang, S. Zheng and Z.-S. Wu, ACS Energy Lett. , 2024, 9, 355–362.
33 S. Mao, Z. Shen, W. Zhang, Q. Wu, Z. Wang and Y. Lu, Adv. Sci., 2022, 9, 2104841.
34 C. Guo, G. Dai, J. Niu, Y. Guo, Z. Sun, H. Chang and Q. Zhang, J. Mater. Res. Technol. 2023, 26, 5860–5872.
35 W.-H. C. Y.-Q. Yan, S. Liu, Y. Ma, J.-H. Luan, Z. Rao, C. Liu, Z.-W. Shan, J. Lu, G. Wu, Science, 2025, 387, 401–406.
36 H. Wan, J. Xu and C. Wang, Nat. Rev. Chem., 2024, 8, 30–44.

View Article Online
DOI: 10.1039/D5EE02060C

37 Q.-K. Zhang, X.-Q. Zhang, J. Wan, N. Yao, T.-L. Song, J. Xie, L.-P. Hou, M.-Y. Zhou, X. Chen, B.-Q. Li, R. Wen, H.-J. Peng, Q. Zhang and J.-Q. Huang, Nat. Energy., 2023, 8, 725–735.
38 L. Wang, J. Yu, S. Li, F. Xi, W. Ma, K. Wei, J. Lu, Z. Tong, B. Liu and B. Luo, Energy Storage Mater., 2024, 66, 103243.
39 S. Yang, T. Meng, Z. Wang and X. Hu, Energy Storage Mater., 2024, 65, 103177.
40 Y. Jin, N.-J. H. Kneusels, L. E. Marbella, E. Castillo-Martínez, P. C. M. M. Magusin, R. S. Weatherup, E. Jónsson, T. Liu, S. Paul and C. P. Grey, J. Am. Chem. Soc., 2018, 140, 9854–9867.
41 Z. He, H. Tu, G. Sun, A. Sun, Y. Wang, J. Sun, G. Wu, W. Li, J. Xu and M. Liu, Adv. Funct. Mater., 2024, 35, 2414569.
42 J. Tang, Y. Zhou, X. Li, X. Huang, W. Tang and B. Tian, Energy Mater., 2024, 4, 400022.
43 Z.-X. Chen, Q. Cheng, X.-Y. Li, Z. Li, Y.-W. Song, F. Sun, M. Zhao, X.-Q. Zhang, B.-Q. Li and J.-Q. Huang, J. Am. Chem. Soc., 2023, 145, 16449–16457.
44 Y.-C. Chien, H. Liu, A. S. Menon, W. R. Brant, D. Brandell and M. J. Lacey, Nat. Commun., 2023, 14, 2289.
45 Y. Peng, M. Ding, K. Zhang, H. Zhang, Y. Hu, Y. Lin, W. Hu, Y. Liao, S. Tang, J. Liang, Y. Wei, Z. Gong, Y. Jin and Y. Yang, ACS Energy Lett., 2024, 9, 6022–6028.
46 Y. Peng, C. Zhong, M. Ding, H. Zhang, Y. Jin, Y. Hu, Y. Liao, L. Yang, S. Wang, X. Yin, J. Liang, Y. Wei, J. Chen, J. Yan, X. Wang, Z. Gong and Y. Yang, Adv. Funct. Mater., 2024, 34, 2404495.
47 W. Wang, F. Xiong, S. Zhu, J. Chen, J. Xie and Q. An, eScience, 2022, 2, 278–294.
48 C. Wang, G. Li, H. Qin, Z. Xiao, D. Wang, B. Zhang, X. Ou and Y. Wu, Adv. Energy Mater., 2022, 12, 2200403.
49 Q. Li, J. Ruan, S. Weng, X. Zhang, J. Hu, H. Li, D. Sun, X. Wang, F. Fang and F. Wang, Angew. Chem. Int. Ed., 2023, 62, e202310297.
50 L. Ye, M. Liao, H. Sun, Y. Yang, C. Tang, Y. Zhao, L. Wang, Y. Xu, L. Zhang, B. Wang, F. Xu, X. Sun, Y. Zhang, H. Dai, P. G. Bruce and H. Peng, Angew. Chem. Int. Ed., 2019, 58, 2437–2442.
51 S. Chen, L. Shen, P. A. van Aken, J. Maier and Y. Yu, Adv. Mater., 2017, 29, 1605650.
52 W. Wu, Y. Kang, M. Wang, D. Xu, J. Wang, Y. Cao, C. Wang and Y. Deng, J. Power Sources, 2020, 464, 228244.
53 Q. Wang, T. Meng, Y. Li, J. Yang, B. Huang, S. Ou, C. Meng, S. Zhang and Y. Tong, Energy Storage Mater, 2021, 39, 354–364.
54 X. Liu, Z. Xu, A. Iqbal, M. Chen, N. Ali, C. Low, R. Qi, J. Zai and X. Qian, Nano-Micro Lett., 2021, 13, 54.
55 Z. -F. Sin, Q. -Z. Yin, S.- G. Zhou, H. -Y. Chen, S. -F. Wen, H. -P. Yang, X. -Y. Wu, J. -H. Pan and Q. -B. Zhang, Adv. Energy Mater., 2025,2500189
56 Y. Yang, Z. Yang, Z. Li, J. Wang, X. He and H. Zhao, Adv. Energy Mater., 2023, 13, 2302068.
57 Z. Cao, X. Zheng, M. Zhou, T. Zhao, L. Lv, Y. Li, Z. Wang, W. Luo and H. Zheng, ACS Energy Lett., 2022, 7, 3581–3592.
58 Y. Yu, C. Yang, Y. Jiang, Z. Shang, J. Zhu, J. Zhang and M. Jiang, Adv. Energy Mater., 2024, 15, 2403086.

View Article Online
DOI: 10.1039/D5EE02060C

Data Availability Statement

The datasets used and analyzed during the current study are available from the corresponding author upon reasonable request.